*17th World Conference on Earthquake Engineering, 17WCEE*
*Sendai, Japan - September 13th to 18th 2020*

# SAFETY EVALUATION PROCEDURES AGAINST BUILDING COLLAPSE DUE TO COLLISION OF TSUNAMI-DRIVEN SHIPS

K. Matsukawa[(1)], D. Kojima[(2)], Y. Haga[(3)] and Y. Nakano[(4)]

[(1)] *Research Associate, Institute of Industrial Science, The University of Tokyo, mtkw@iis.u-tokyo.ac.jp*
[(2)] *East Japan Railway Company, kojima-d@jreast.co.jp*
[(3)] *Senior Collaborator, Institute of Industrial Science, The University of Tokyo, y-haga@iis.u-tokyo.ac.jp*
[(4)] *Professor, Institute of Industrial Science, The University of Tokyo, iisnak@iis.u-tokyo.ac.jp*

## *Abstract*

Massive tsunami-driven debris such as ships can cause critical damage the buildings by colliding to their columns and it possibly leads building collapse because of induced decrease in axial load carrying capacity. The Ministry of Land, Infrastructure, Transport and Tourism issued the "Interim Guidelines on the Structural Design of Tsunami Evacuation Buildings" in November 2011. These guidelines contain quantitative safety evaluation procedures for buildings against tsunami load; however, they do not quantitatively consider the influence of debris collisions. Therefore, the authors propose quantitative safety evaluation procedures to prevent building collapse based on the residual axial load-carrying capacity of damaged columns. The final part of these procedures is a safety evaluation, during which the acting axial load and the residual axial load-carrying capacity are compared at the maximum lateral displacement; several existing models for the residual axial load-carrying capacity of columns that are a function of lateral displacement can be used in this part. In the initial part of these procedures, the maximum column displacement $\delta_{max}$ is estimated using the law of the conservation of energy and given parameters, including the mass of the ship $m_s$, the drifting velocity of the ship $v_s$ and the shear strength of the column $V_{static}$. However, the coefficient of restitution $e$, the efficiency factor of energy transfer from the ships to the columns $f_e$, the dynamic strength increase factor due to a higher strain rate $\alpha$, and the modification factor $\beta$ used to convert load-displacement curves into equivalent rectangular shapes were previously unknown. Thus, the authors experimentally investigated these values. The experiment was performed using a pendulum system built at a 1/10 scale, and the steel pendulum was carefully designed to be equivalent to steel ships in terms of length, weight and bow curvature. The mass (steel bars) collided with the vertical center of the reinforced concrete column specimens, which were fixed at both ends. The following conclusions were drawn from this study: (1) the coefficient of restitution $e$ ranged from 0.13 to 0.3 and converged to approximately 0.2 except for the weakest collision cases; (2) approximately 75% of the kinetic energy of the steel mass was transferred to the column ($f_e$ = 0.75); (3) the dynamic strength increase factor of the column due to a higher strain rate ranged from 1.6 to 1.7, and these values were close to those of concrete materials identified in the CEB-FIP model; and (4) the modification factor $\beta$ was calculated to be approximately 0.8.

*Keywords: tsunami, debris, reinforced concrete, column, residual axial load-carrying capacity*



## 1. Introduction

In past tsunami events, such as the 2011 Great East Japan Earthquake, a great amount of debris was observed, and this debris was driven deep into inland areas. Massive debris, such as ships, can cause critical damage to buildings when colliding with their vertical load-bearing members, such as columns; these events can potentially lead to building collapse because of the induced decrease in axial load-carrying capacity. Fig. 1 [1] shows an example of building collapse caused by a collision with a tsunami-driven ship, which was observed after the 2011 earthquake. The Ministry of Land, Infrastructure, Transport and Tourism of Japan issued the "Interim Guidelines on the Structural Design of Tsunami Evacuation Buildings" [2] in November 2011. These guidelines contain quantitative safety evaluation procedures for buildings against tsunami loads; however, these guidelines do not quantitatively consider the influence of debris collisions.

Fig. 1 An example of building collapse due to tsunami-driven ship collisions [1]

Asai et al. studied the lateral responses of building structures induced by tsunami-driven ship impact loads under the assumption that the ships collide with hard and rigid floor slabs [3, 4]. However, they did not account for their collisions on vertical members, such as columns, or the possibility of collapse due to a decrease in their axial load-carrying capacity. Therefore, in this paper, the authors perform a collision test using reinforced concrete (RC) column specimens and pendulums, and propose quantitative safety evaluation procedures to prevent building collapse based on the test results.

## 2. Proposal of safety evaluation procedures

Figs. 2 and 3 show a whole safety evaluation procedure and detailed procedures up to response displacement estimation, respectively. In this process, first, the maximum column lateral displacement $\delta_{max}$ due to collision must be estimated using the equilibrium of energy and given parameters, such as the mass of the ship $m_s$, the drifting velocity of the ship $v_s$ and the static shear strength of the column $V_{static}$. Eq. (1) is used to calculate the energy transferred from the ship during collisions $\Delta E$ and is derived assuming 1) the law of the conservation of energy, 2) the zero velocity of the building before the collision.

$$\Delta E = \frac{1}{2} m_s v_s^{\,2} - \frac{1}{2} m_s v'^{\,2}_s \tag{1}$$

where $v'_s$ is the ship velocity after collision ($=e \cdot v_s$) and $e$ is the coefficient of restitution.

Here, the energy transferred to the columns $E_a$ is represented by Eq. (2).

$$E_a = f_e \cdot \Delta E \tag{2}$$

where $f_e$ is the efficiency factor of the energy transfer from the ships to columns, which will be discussed later.



 



When the column deforms due to a ship collision, energy absorption occurs, and this absorbed energy is defined as the area of the load-displacement curve and is considered equivalent to the energy transferred to the column $E_a$. The area is calculated by converting the shape of the load-displacement curve into an equivalent rectangle using the factor $\beta$, as shown in Fig. 3. The dynamic maximum load $F_{dyn}$ is estimated using the static maximum strength $V_{static}$ under static loading and the dynamic strength increase factor $\alpha$, as shown in Eq. (3). This equation is derived from the assumptions that ships collide at the vertical center of the column and that both upper and lower parts fail simultaneously (therefore $V_{static}$ of both upper and lower parts are considered, as shown in Eq. (3).).

$$F_{dyn} = 2 \cdot \alpha \cdot V_{static} \tag{3}$$

Then, the maximum lateral response displacement of the column $\delta_{max}$ can be determined from the converted rectangular shape and the energy transferred to the column $E_a$, as shown in Eq. (4).

$$\delta_{max} = \frac{E_a}{\beta \cdot F_{dyn}} \tag{4}$$

The rest of the procedures are the safety evaluations using the axial load acting on the column $P$ and the residual axial load-carrying capacity of the column $P_R$, which is a function of the obtained $\delta_{max}$. Several existing models, such as those proposed by Elwood and Mohele [5] and Yang et al. [6, 7], are available to calculate $P_R$ using $\delta_{max}$. Then, the safety evaluation could end with a comparison of the acting axial load $P$ and the residual axial load-carrying capacity $P_R$. However, in the procedures above, the coefficient of restitution $e$, the efficiency factor of energy transfer from the ships to the columns $f_e$, the dynamic strength increase factor due to higher strain rates $\alpha$, and the factor $\beta$ used to convert the load-deflection curves into an equivalent rectangular shape are not known so far. Therefore, the authors experimentally investigated these values.

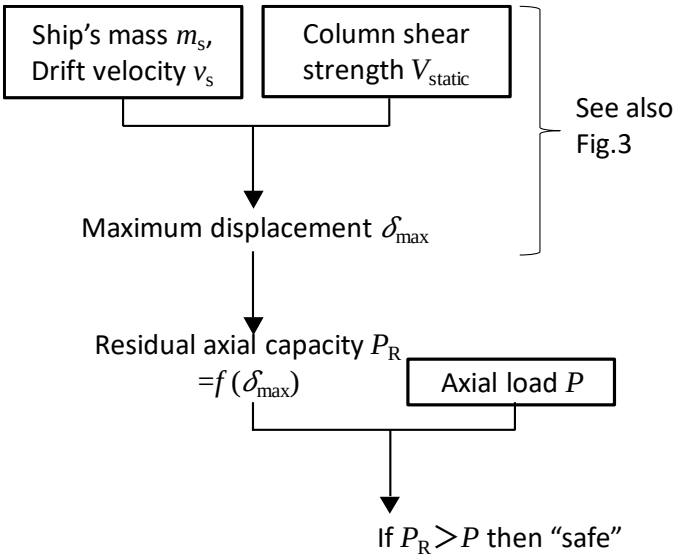


Fig. 2 Safety evaluation procedures



 



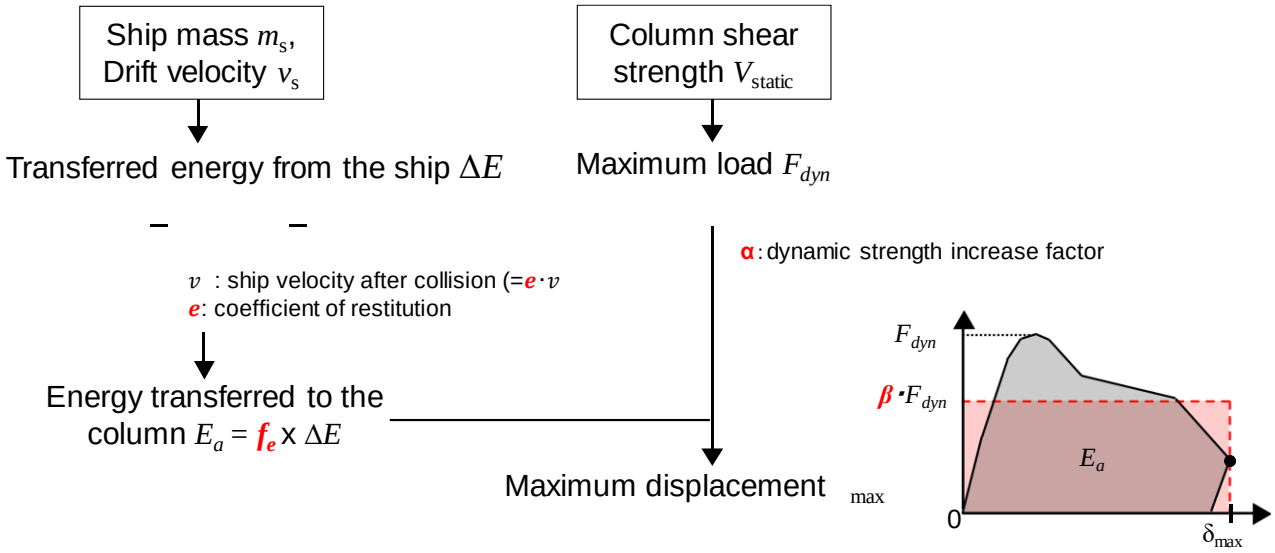


Fig. 3 Detailed procedures up to maximum displacement estimation

## 3. Collision test using a pendulum system

### 3.1 Test program

#### 3.1.1 Design of the pendulum

The collision tests were carried out using a pendulum system. The scale of the test was 1/10. Eight steel bars were designed to reproduce the displacement tonnage (equal to $m_s$), length of the ship and the curvature of its bow. The displacement tonnages (equal to $m_s$) of the target ships were first determined, ranging from 2.5 tons (small ship) to 60.0 tons (medium ship). Their lengths were calculated from a correlation with gross tonnage, which is an index of ship volume and can be calculated from their displacement tonnages [3]. These steel bars were hung on wire ropes so that the bars could hit the vertical center of the specimens, as shown in Fig. 4. The velocity upon collision was controlled by the height of the initial position of the pendulum. The identified height (1,837 mm) in Fig. 4 was used to reproduce the 6 m/s (The target velocity is basically 6 m/s, which is derived from flow velocity observed in the 2011 tsunami [8].) velocity for the collision.

#### 3.1.2 Column specimen

A total of eighteen RC column specimens were manufactured. Twelve of the eighteen specimens were designed to fail in flexure under the loading conditions (loaded on the vertical center of the column with its both ends fixed), whereas the remaining specimens were designed to fail in shear. Most of the specimens were made as only the column body without stub; however, several specimens were designed with stub portions at both ends (see Fig. 5) so that the fixed condition at both end of a column mentioned above was certainly reproduced. The combinations of columns and colliding steel bars are listed in Table 1. In addition, several identical specimens (not shown in Table 1) were manufactured for each type of column specimen and tested under static load to investigate the dynamic strength increase factor $\alpha$.



 



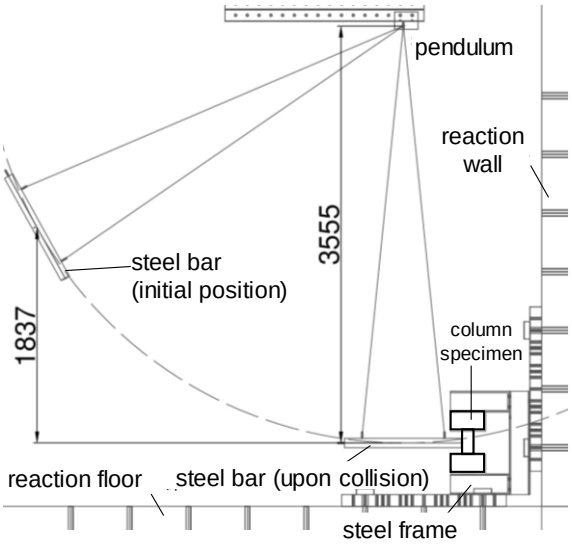


Fig. 4 Collision test setup (unit: mm)

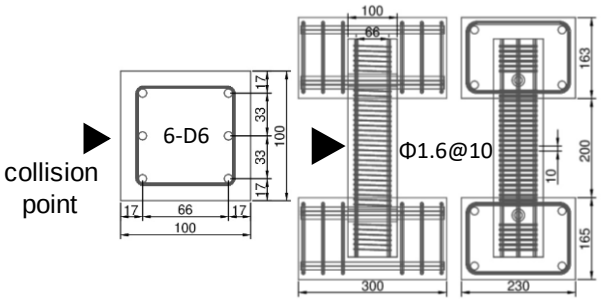


Fig. 5 A specimen with stub portions (unit: mm)

Table 1. Combinations of column specimens and colliding steel bars

| Column specimens | | Colliding steel bars | | |
|---|---|---|---|---|
| Failure type | Name | Name<br>Φ + dia.(mm) - length(mm) | Target velocity upon collision [m/s] | $m_s$ [kg] |
| Shear failure type (with stubs) | SS-1 | Φ80-1000 | 6.0 | 39.55 |
| | SS-2 | Φ100-1000 | | 61.55 |
| | SS-3 | | | |
| Shear failure type (without stubs) | S-8 | Φ50-1000 | | 15.35 |
| Flexural failure type (without stubs) | B-1 | Φ19-1000 | | 2.20 |
| | B-2 | Φ28-1000 | | 4.85 |
| | B-3 | Φ50-1000 | | 15.35 |
| | B-4 | | 3.0 | |
| | B-5 | Φ60-1000 | 6.0 | 22.10 |
| | B-6 | Φ28-750 | | 3.60 |
| | B-7 | Φ32-750 | | 4.70 |
| | B-8a | Φ50-1000 | | 15.35 |
| | B-8b | | | |
| | B-9a | Φ60-1000 | | 22.10 |
| | B-9b | | | |



 



### 3.1.3 Loading and measurement

As previously mentioned, the collision velocity was planned to be basically 6 m/s (only one specimen, B-4 was subjected to a collision at a velocity of 3 m/s for comparison). A high-speed camera with a frame rate of 10,000 FPS was used for measurement. The displacement time history of the steel bars was first obtained from digital image analysis (using pixel-per-length) of tracking marks that were placed on the top of the steel bars. The velocity and acceleration were then computed from the time derivatives of the displacement time history. The horizontal displacement of the column was measured at the vertical center of the column with displacement transducers. However, for all specimens, the displacement transducers could not capture the specimen deformation after reaching the maximum strength. Therefore, the time history of the specimen displacement after maximum strength was obtained using digital image correlation software only for the specimens tested in the later phase of the experiment: specimens SS-1, SS-2 and SS-3. The digital image correlation software was also used to compute the strains for the determination of the strain rate.

## 3.2 Test results

The results are shown in Table 2. Because the displacement time history of the steel bar, which was obtained from the pixel-per-length, contains noise caused by minor inaccuracies in image tracking, a 1000 Hz low pass filter was used to eliminate the noise, as shown in Fig. 6. The impact load was obtained as the product of the ship mass $m_s$ and the filtered acceleration. Here, the starting and ending times at collision were defined as the times at which the acceleration value first crosses 0 m/s on the time history before and after the maximum acceleration was observed, respectively, as shown in Fig. 6. Then, the coefficient of restitution $e$ was calculated using the velocity at both the collision start ($v_s$) and end ($v'_s$). In this section, the representative cases, SS-1, SS-2, SS-3 and B-1, are mentioned in detail.

Table 2. Test results

| Column specimen name | $v_s$ [m/s] | $v'_s$ [m/s] | $e$ | $F_{dyn}$ [kN] | $V_{static}$ [kN] | $\alpha$ | $E_a$ by Eq.(5) [kN·mm] | $\delta$ at $F_{dyn}$ [mm] | $\delta_{max}$ [mm] | Note |
|---|---|---|---|---|---|---|---|---|---|---|
| SS-1 | 6.1 | -1.6 | 0.26 | 141 | 90 | 1.56 | 523 | - | 4.53 | |
| SS-2 | 5.7 | (-1.1) | (0.19) | (126) | | (1.40) | (818) | - | (7.84) | Steel bar touched the nuts during collision. The values within the brackets are only for reference. |
| SS-3 | 6.1 | -1.2 | 0.19 | 157 | | 1.74 | 830* | - | 6.90 | *$E_a$ was estimated as mentioned in Section 4.1. |
| S-8 | 6.2 | -1.4 | 0.23 | 101 | 72 | 1.41 | 145** | 1.71 | - | **$E_a$ was calculated using the load-displacement curve up to the maximum impact load. |
| B-1 | 6.1 | -3.4 | 0.55 | 29 | 55 | 0.53 | 14** | 0.55 | - | |
| B-2 | 6.1 | -0.8 | 0.13 | 49 | | 0.89 | 51** | 1.22 | - | |
| B-3 | 5.9 | -1.3 | 0.21 | 78 | | 1.43 | - | - | - | |
| B-4 | 3.0 | -0.9 | 0.29 | 54 | | 0.99 | 37** | 0.75 | - | |
| B-5 | 5.7 | -1.3 | 0.24 | 91 | | 1.67 | - | - | - | |
| B-6 | 6.0 | -0.8 | 0.14 | 40 | | 0.74 | 33** | 0.99 | | |
| B-7 | 6.1 | -0.6 | 0.10 | 50 | | 0.90 | 32** | 0.74 | - | |
| B-8a | 5.9 | -1.6 | 0.28 | 77 | | 1.40 | 126** | 1.72 | - | |
| B-8b | 5.7 | -1.6 | 0.27 | 70 | | 1.28 | 118** | 1.85 | - | |
| B-9a | 5.7 | -1.7 | 0.30 | 86 | | 1.57 | 158** | 2.04 | - | |
| B-9b | 5.8 | -1.6 | 0.27 | 90 | | 1.64 | 130** | 1.56 | - | |



 



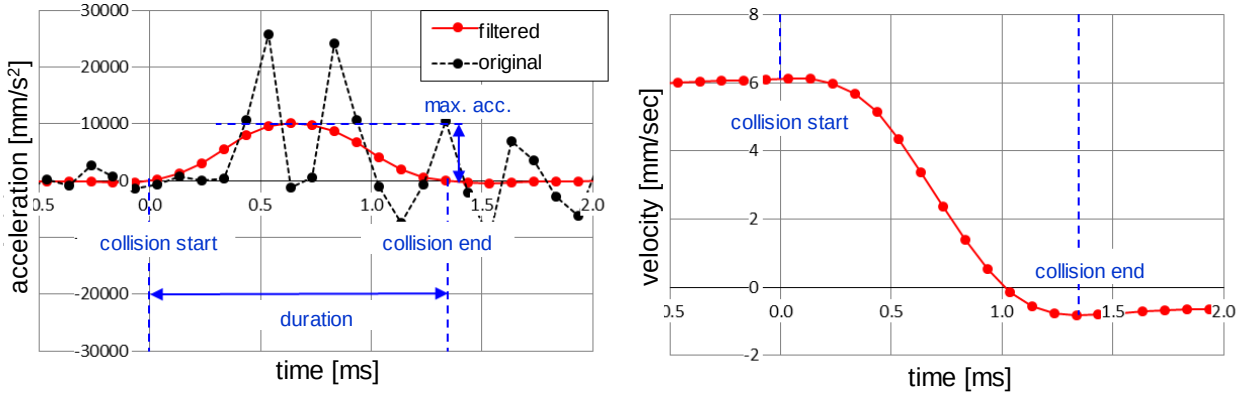


Fig. 6 Definition of collision start/end in the acceleration and corresponding velocity time history

(a) Specimen SS-1

In this specimen, $v_s$ and $v_s$' were 6.1 m/s and -1.6 m/s, respectively, whereas the coefficient of restitution $e$ was 0.26. The maximum displacement at the vertical center $\delta_{max}$ was 4.53 mm. The maximum impact load $F_{dyn}$ was 141 kN, and the increment ratio from the static maximum load ($V_{static}$) was 1.56. The pictures and load-displacement curve of this specimen are shown in Fig. 7.

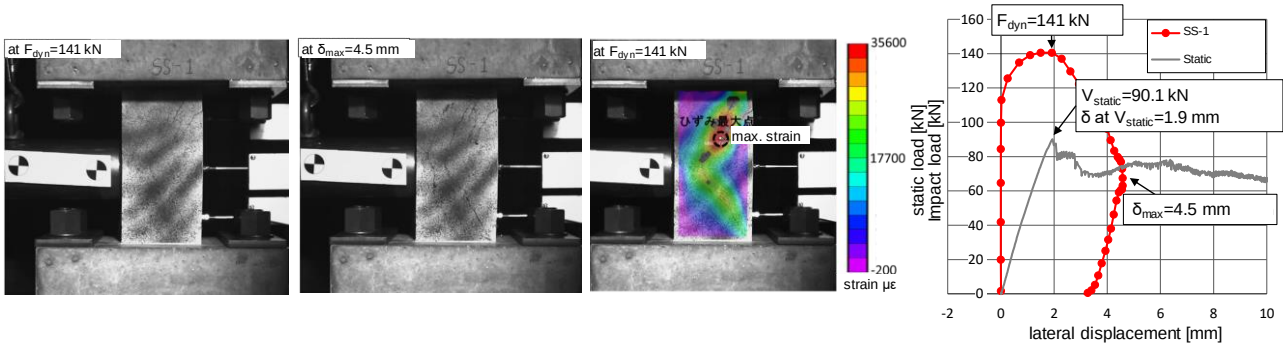


Fig. 7 Pictures and load-displacement curve of specimen SS-1

(b) Specimen SS-2

During the collision, steel bars touched the nuts used to fix the specimen. Therefore, the results of this specimen were treated exclusively and shown as a reference.

(c) Specimen SS-3

The maximum displacement was not measured with the digital image correlation software because of the formation of a large diagonal crack. Thus, the authors manually calculated the maximum displacement using pixel-per-length information and a picture that corresponded to the occurrence of the maximum displacement; the result from this procedure was 6.9 mm. The unloading stiffness was estimated to be the same as the secant modulus at which the maximum impact load was measured. The load-displacement curve, including the estimated curve, is shown in Fig. 8 (estimated parts are shown as dotted lines).



 



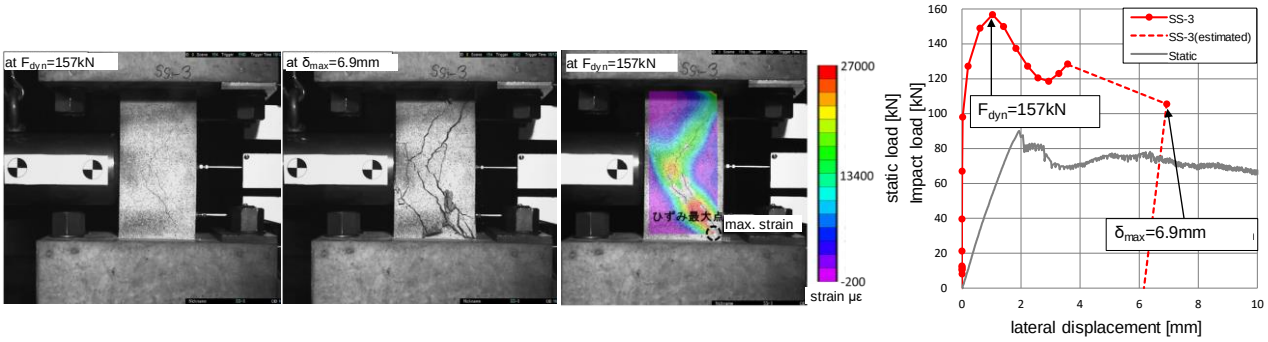


Fig. 8 Pictures and load-displacement curve of specimen SS-3

(d) Specimen B-1

For specimen B-1, the displacement transducer could not capture the momentary displacement reversal after $F_{dyn}$, as shown in Fig.9. Therefore the displacement data after $F_{dyn}$ was not obtained. However, $F_{dyn}$, $v_s$ and $v_s$' were obtained because these are independent from the transducers. $F_{dyn}$ was 29.1 kN. $v_s$ and $v_s$' were 6.1 m/s and -3.4 m/s, respectively, whereas the coefficient of restitution $e$ was 0.55. Unlike Figs. 7 and 8, $F_{dyn}$ is smaller than static test result, because the lightest steel bar is collided and it did not cause any substantial damage. Therefore the coefficient of restitution $e$ was higher than other specimens.

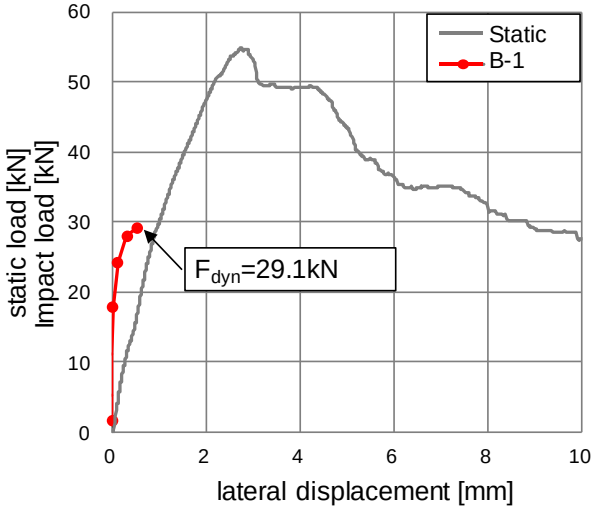


Fig. 9 Load-displacement curve of specimen B-1

## 4. Resulted values for safety evaluation

### 4.1 Efficiency factor of energy transfer from ships to columns $f_e$

The efficiency factor of energy transfer from ships to columns $f_e$ was calculated as the ratio of $\Delta E$ to $E_a$, according to Eq. (2). From the test data, $\Delta E$ was calculated using Eq. (1), and $E_a$, which corresponds to the area of the load-displacement curve of the column (energy absorbed by column), was calculated using Eq. (5).

$$E_a = \int (F \cdot \delta) d\delta \tag{5}$$



 



For column SS-3, the area enclosed by the solid line (measured part) and dotted line (estimated part) shown in Fig.8 was used, whereas for the S-type and B-type specimens, the area was calculated up to the maximum impact load and was only used as reference here. The relationship between $\Delta E$ and $E_a$ is shown in Fig. 10. A nearly linear relationship can be found, and approximately 75% of the energy was transferred to the column. Therefore, the value of $f_e$ from this study was 0.75.

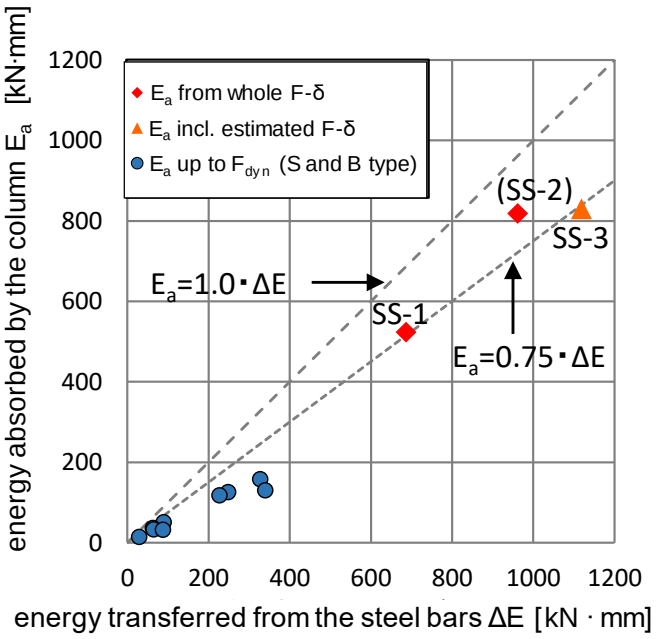


Fig. 10 Efficiency factor of energy transfer

### 4.2 Coefficient of restitution *e*

Under the assumption that the velocity of the building before the collision is equal to zero, the coefficient of restitution can be calculated with Eq. (6), which was derived from the laws of conservation of momentum and conservation of mechanical energy. The value $e$ was plotted with respect to the kinetic energy $1/2 m_s v_s^2$, as shown in Fig. 11.

$$e = \sqrt{1 - \frac{\Delta E}{\frac{1}{2} m_s v_s^2}} \tag{6}$$



 



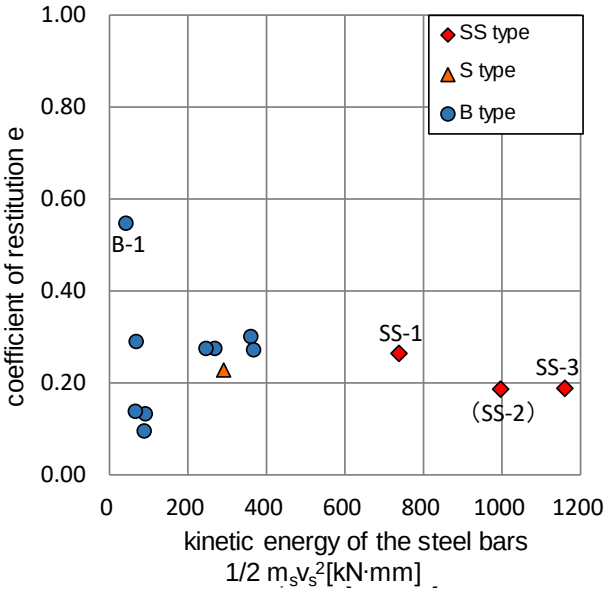


Fig. 11 Coefficient of restitution *e*

Although the specimen B-1, which collided with the smallest kinetic energy, exhibited the highest *e* (=0.55), *e* in other specimens ranged from 0.13 to 0.30 and converged to approximately 0.2 as the kinetic energy increased.

### 4.3 Dynamic strength increase factor due to a higher strain rate *α*

The relationship between the strain rate and dynamic strength increase factor of the RC columns is shown in Fig. 12 [9]. The obtained strain rates ranged from $10^1$ to $10^2$ $s^{-1}$, where a drastic change in the dynamic increase factor was observed according to the CEB-FIP model [10]. The dynamic strength increase factor of the specimens was approximately 1.6 or 1.7, which was in good agreement with the CEB-FIP model.

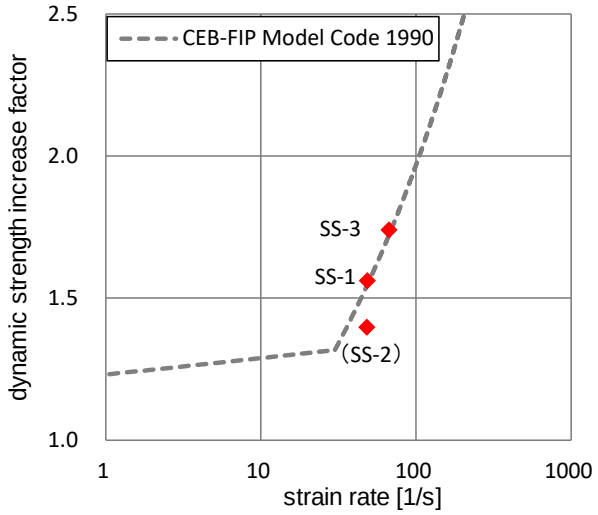


Fig. 12 Relationship between the strain rate and dynamic strength increase factor [9]



 



### 4.4 Factor to convert a load-displacement curve into an equivalent rectangular shape $\beta$

As mentioned in section 2, the load-displacement curve of the column must be converted into an equivalent rectangular shape to calculate the maximum lateral displacement $\delta_{max}$ using $E_a$ and $F_{max}$, as shown in Fig. 13. When the value $\beta$ is known from experiments, $\delta_{max}$ can be estimated even though the load-displacement curve is unknown (such as structural design). From the series of tests shown in this paper, the factor $\beta$ ranged from 0.80 to 0.95. In specimen SS1, for which the load-displacement curve was fully used to calculate $E_a$, the value of $\beta$ was approximately 0.80. However, as shown in Fig. 14, when the shape of the load-displacement curve of the general shear column was assumed to be triangular, the value of $\beta$ was expected to be 0.5. The test results showed higher values than expected. The suggested reason for this discrepancy was that the axial load, which is one of the dominant factors for the capacity deterioration after shear failure, was not applied to these column specimens. Therefore, further experimental studies applying axial loads are needed to obtain a reasonable value for $\beta$.

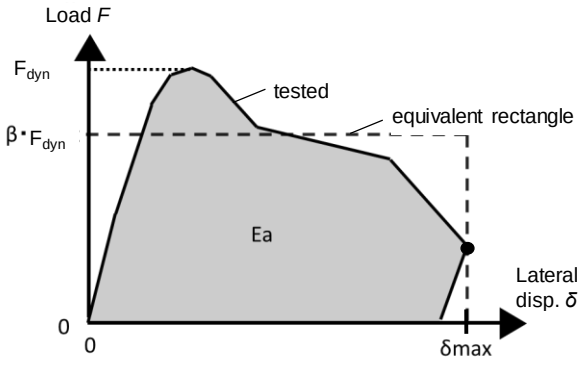


Fig. 13 Conversion into an equivalent rectangular shape

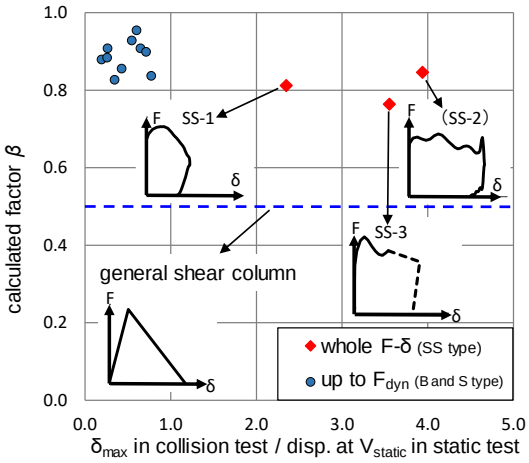


Fig. 14 Obtained $\beta$ values from the tests

## 5. Conclusions

In this study, the coefficient of restitution $e$, the efficiency factor of energy transfer from ships to columns $f_e$, the dynamic strength increase factor due to a higher strain rate $\alpha$, and the modification factor $\beta$ used to convert load-displacement curves into equivalent rectangular shapes were investigated through a series of collision tests for the purpose of developing a safety evaluation method to prevent building collapses induced by tsunami-driven debris. The key findings from this study are listed hereafter:

(1) The energy absorbed by the column $E_a$ was found proportional to the energy transferred from the ship during a collision $\Delta E$ and its ratio, the efficiency factor of the energy transfer $f_e$, was approximately 0.75

(2) The coefficient of restitution $e$ ranged from 0.13 to 0.30, and these values converged to approximately 0.2 as the kinetic energy of the steel bar increased.

(3) The dynamic strength increase factor $\alpha$ of the specimens was approximately 1.6 or 1.7, which was in good agreement with the CEB-FIP model.

(4) The value of $\beta$ was expected to be approximately 0.5 considering the general load-displacement curve of the column prone to shear failure. However, because the test was performed without the application of axial loads, the drastic capacity deterioration after shear failure was not clearly observed. Therefore, the value of $\beta$ in this test was 0.8, which was higher than expected.



 




## Acknowledgments

This work was supported by JSPS KAKENHI Grant Number JP18H01581 (Principal Investigator: Yoshiaki Nakano). The authors would like to express their gratitude to the support.

## References

[1] Port and Airport Research Institute, Japan, *Technical Note of the Port and Airport Research Institute*, No.1231, Yokosuka, 2011

[2] MLIT/Ministry of Land, Infrastructure, Transport and Tourism, Japan (2011): *Interim Guidelines on Structural Requirements for Tsunami Evacuation Buildings Considering the Great East Japan Earthquake. Annex to the Technical Advice*, MLIT, Housing Bureau, Building Guidance Division, No. 2570. (in Japanese)

[3] Asai, T., Matsukawa, K., Choi, H. & Nakano, Y. (2015): Response Estimation Method of Buildings due to Waterborne Debris Impact Loads. *10th Pacific Conference on Earthquake Engineering*, Sydney, Australia.

[4] Asai, T., Matsukawa, K., Choi, H. & Nakano, Y. (2017): Simplified Response Estimation Method of Buildings due to Tsunami-Driven Ship Impact Loads. *16th World Conference on Earthquake*, Santiago, Chile.

[5] Elwood KJ & Moehle JP (2005): Axial capacity model for shear-damaged columns. *ACI Structural Journal*, **102**(4), 578–587.

[6] Yang, Y., Matsukawa, K., Choi, H., & Nakano, Y. (2019). Study of the residual axial capacities of shear-damaged reinforced concrete columns: Part 1—development of an evaluation model. *Advances in Structural Engineering*, 22(2), 311–322.

[7] Yang, Y., Matsukawa, K., Choi, H., & Nakano, Y. (2019). Study of the residual axial capacities of shear-damaged reinforced concrete columns: Part 2—experimental verification of an evaluation model. *Advances in Structural Engineering*, 22(2), 459–472.

[8] Asai, T., Nakano, Y., Tateno, T., Fukuyama, H., Fujima, K., Sugano, T., Haga, Y., Okada, T. (2012), Tsunami Load Evaluation Based on Field Investigations of the 2011 Great East Japan Earthquake, *15th World Conference on Earthquake*, Lisbon, Portugal.

[9] Kojima, D. (2019), Fundamental Study on the Safety Evaluation Method of Reinforced Concrete Column against Collision of Tsunami-Driven Ships., Master Thesis, The University of Tokyo.(in Japanese) (The title of this thesis was translated by the author of this paper)

[10] CEB-FIP Model Code 1990 (1993).



 